Application of SeDDaRA Blind Deconvolution for Efficient Improvement of Confocal Microscopy Images

Dr. James N. Caron
Quarktet, 205 Indian Spring Drive, Silver Spring, MD 20901, U.S.A.
http://www.Quarktet.com
caron@quarktet.com

February 2, 2011

Abstract

This paper presents the application of the SeDDaRA blind deconvolution method to image sequences produced by confocal microscopy. In contrast to more common methods, such as Lucy-Richardson and maximum entropy, SeDDaRA is non-iterative. As such, this approach requires significantly less computation while still producing significant blur reduction. Based on scene-statistics, successful application of this method results from finding a suitable representation of the scene, as opposed to deriving a reasonable model of the point spread function. The method is described and applied to two distinct confocal image stacks that are available from the National Institute of Health web site. A resolution-based image metric, derived from the full-width half-maximum values of image features, is applied to assess image improvement. Based on visual inspection and the image metric, the processed image sets show significant improvements in image resolution and contrast.

1 Introduction

Confocal microscopy has developed into a standard research tool for studying cell biology. Using a combination of pinholes and mirrors, confocal microscopy limits single image capture to the focal plane of the microscope, eliminating out-of-focus light. In operation, an image is captured for each optical depth containing only the elements that are in focus, producing an 'image stack.' The image stack can be presented as a three-dimensional representation of the sample, or as a high-resolution two-dimensional image produced by averaging the image stack. However, confocal microscopes still can possess chromatic and spherical optical aberrations, creating blur and reducing resolution in the captured images.

To remove the blur in post-processing, researchers have applied iterative blind deconvolution methods such as Richardson-Lucy, [1, 2] maximum likelihood, [3], a customized minimization algorithm. [4], and the Gold-Meinel technique. [5] In this study, we applied the SeDDaRA method to confocal image stacks and report the improvement using image resolution as the metric. SeDDaRA is an effective non-iterative deconvolution process that has been applied to solar imaging, [6] turbulence-degraded images, [7] SEM imaging, [8] and retinal scanning. [9] Since the method is non-iterative, it saves on processing time while effectively de-blurring the image. The objective of this paper is to apply the SeDDaRA method to image stacks created by confocal microscopy and measure improvement using the full-width half-maximum values of image features.

2 SeDDaRA Deconvolution

The Self-Deconvolving Data Reconstruction Algorithm (SeDDaRA), [10] is based on the premise that there is enough knowledge of the scene statistics that a suitable model of the scene can be found. Thus, a reference image with similar spatial frequency content, but no blur, is used as a model to extract the blur from the target image.

The mathematical representation of the blurred image $g(x, y)$ is

$$g(x, y) = f(x, y) \circ d(x, y) + w(x, y) \tag{1}$$

where $f(x, y)$ is the real scene, $d(x, y)$ is the point spread function (PSF), $w(x, y)$ is a noise term, and '$\circ$' indicates convolution. The objective of blind deconvolution is to find the best estimate of $f(x, y)$ from $g(x, y)$ when $d(x, y)$ and $w(x, y)$ are unknown. Application of a fast Fourier transform (FFT) produces

$$G(u, v) = F(u, v)\ D(u, v) + W(u, v) \tag{2}$$

where (u, v) are the coordinates in frequency space, and the transformed functions are represented by capital letters.

If $d(x, y)$ is known, a deconvolution process can be applied to $g(x, y)$ to estimate $f(x, y)$. Many suitable deconvolution algorithms, such as non-negative least squares and the Wiener filter, can be found in the literature. [11, 12, 13, 14] For this effort, a pseudo-inverse filter, an approximation of the Wiener filter, has been used. It is a fast process and very robust, and has been shown as effective as iterative deconvolution approaches. [15, 16] The deconvolution is given by

$$F(u, v) \approx \frac{G(u, v)\ D^*(u, v)}{|D(u, v)|^2 + C_2} \tag{3}$$

where the parameter C_2 is typically chosen as 0.01 multiplied by the average of $|D(u, v)|$. The constant acts as a tuning parameter to guard against amplification of the image noise.

Without explicit knowledge of $d(x, y)$, the function must be estimated through blind deconvolution. Research on blind deconvolution extends back several

decades, but studies by Ayers and Dainty [17] spurred an increase in activity in the astronomical community [18]. All methods require some prior knowledge of either the scene, [19] the scene statistics, [3, 20] or the shape of the blur function. [21] Many of these techniques are iterative and can only be applied within certain restraints. In contrast, the SeDDaRA approach can be applied to a large range of scene types. [10]

The SeDDaRA process assumes the PSF is space-invariant and has the form

$$D(u,v) = [K_G \mathcal{S}\{|G(u,v) - W(u,v)|\}]^{\alpha(u,v)} \tag{4}$$

where $\alpha(u,v)$ is a tuning parameter and K_G is a real, positive scalar chosen to ensure $|D(u,v)| \leq 1$. Application of the smoothing filter $\mathcal{S}\{...\}$ assumes that $D(u,v)$ is a slowly varying function. Assumptions for this calculation are explained in reference [10].

After some derivation, $\alpha(u,v)$ is found to be

$$\alpha(u,v) \approx \frac{\mathrm{Ln}[K_G \mathcal{S}|G(u,v) - W(u,v)|] - \mathrm{Ln}[K_{F'} \mathcal{S}\{|F'(u,v)|\}]}{\mathrm{Ln}[K_G \mathcal{S}|G(u,v) - W(u,v)|]} \tag{5}$$

where $F'(u,v)$ is a reference image that satisfies

$$K_{F'} \mathcal{S}\{|F'(u,v)|\} \approx K_F \mathcal{S}\{|F(u,v)|\}. \tag{6}$$

The presence of a smoothing filter greatly relaxes this condition. In Equation 5, K_G and $K_{F'}$ must be determined such that $|D(u,v)| \leq 1$. This condition is satisfied if we set $K_G = 1/\mathrm{Max}[\mathcal{S}\{|G(u,v)|\}]$ and $K_{F'} = 1/\mathrm{Max}[\mathcal{S}\{|F'(u,v)|\}]$.

However, as first reported in Reference [22], SeDDaRA can be approximated by expressing $\alpha(u,v)$ as a constant of frequency α. The value α depends on scene statistics, but often $\alpha = 0.5$ is an appropriate choice. The constant-frequency approximation is often as effective as Equation 5, particularly when the PSF has rotational symmetry.

Once $D(u,v)$ has been extracted from the averaged image, both functions are inserted into Equation 3 to remove the blur. Application of an inverse FFT produces the restored image.

3 Description of Image Metrics

With blind deconvolution, absolute measurements of image improvement can only be made if a non-blurred image stack exists. In practical situations, and for the cases studied here, the truth images cannot be obtained. Thus, standard image processing metrics such as Mean-Square-Error and Signal-to-Noise measures [23] cannot be applied.

Instead, the effectiveness of the algorithm is based on the improvement in image resolution as measured by the full-width half maximum (FWHM) of image features. [24, 25]. In this approach, profile plots are extracted across sixteen small peaks in the original and processed images. The average of the FWHM

from each peak is calculated. The amount of improvement can then be expressed either in pixels [8]

$$I = FWHM_{after} - FWHM_{before} \tag{7}$$

or as a ratio,

$$I_{ratio} = \frac{FWHM_{before} - FWHM_{after}}{FWHM_{before}}. \tag{8}$$

producing a reasonable assessment of the improvement in resolution. The disadvantage of this method is that it is scene-dependent and cannot be considered an absolute metric.

The metric was tested by processing a fractal image that was convolved with an out-of-focus PSF, extracted using SeDDaRA from a blurry image. Fractal images are created using mathematical formulae, producing nature-like images with perfect focus. The gray-scale fractal without and with blur is shown in Figure 1. Using the same PSF, the pseudo-inverse filter was applied while varying the C_2 constant. The FWHM metric was then applied to the image features, with the results shown in Figure 2. The plot shows improving image quality with decreasing C_2 while leveling off at $C_2 = 0.05$. The slight decrease appears to be the result of the amplification of noise introduced by using the real PSF. Application of the metric to the non-blurred produced $I_{ratio} = 0.490$.

4 Application

Two image stacks were acquired from the National Institute of Health website for the ImageJ program. [26] We chose to use public-domain image stacks to allow direct comparisons with other blind deconvolution techniques. To the best of our knowledge, no direct comparisons between methods has been published for confocal microscopy. With this approach, other researchers will be able to make direct comparisons with this work.

The images were processed by applying blind deconvolution in two ways, first to the collapsed image, and second to individual frames. The resulting image stack from the latter was collapsed to provide a direct comparison between the two approaches.

4.1 Image Stack Alpha

The first set, called confocal stack and designated here as stack alpha, consisted of 36 layers, with each focal depth layer having an 8-bit red image and an 8-bit green image. The image blur is not very apparent, as shown in the collapsed view (average of all frames) in Figure 3 (top).

The stack was processed by application of SeDDaRA and the constant-frequency approximation on both single frames and the collapsed image. For the SeDDaRA processing, a 512 by 512 fractal image, shown in Figure 4, was chosen as the reference image and the C_2 scaling factor was set to 0.006. For

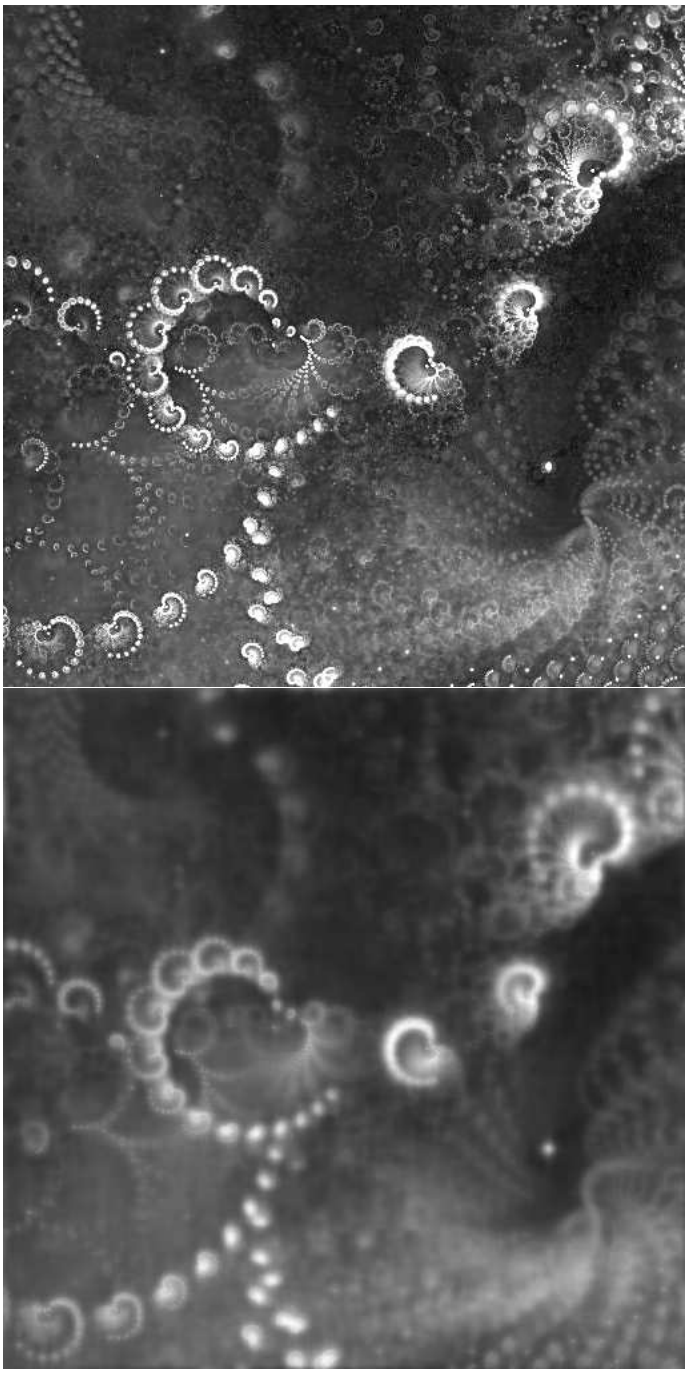

Figure 1: (Top) A fractal image used in the test case for the applying the IFWHM metric. (Bottom) The fractal image was convolved with a real out-of-focus PSF to create a simulated blurred image. Repeated deconvolution of the blurred image, while varying the C_2 scaling factor, produce a set of images with a range of blur.

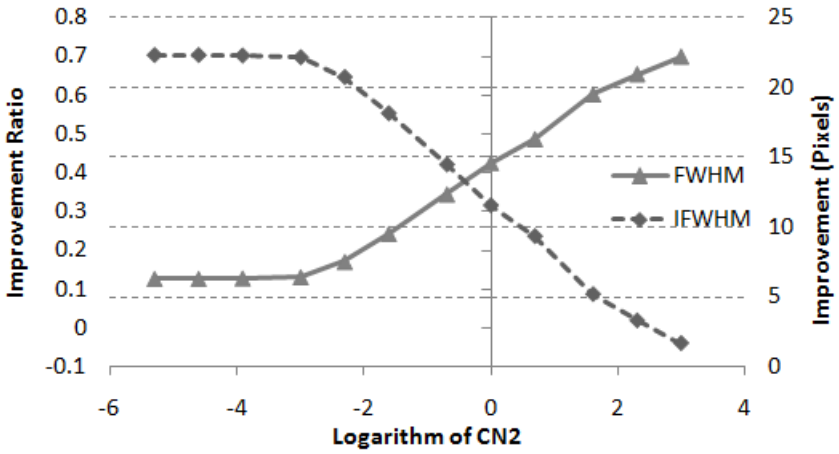

Figure 2: The averaged FWHM values and the I_{ratio} metric plotted as a function of the logarithm of the C_2 scaling factor in the pseudo-inverse filter. Lower values of the scaling factor produce less blur, which decrease the FWHM value of image features. The improvement plateaus as the C_2 scaling factor reaches 0.05.

the constant-frequency approximation, α was set to 0.4 and C_2 scaling factor was set to 0.01. The result of a single frame is shown in Figure 5.

The FWHM metric was applied to both the red and green frames, with the results shown in Table 1. The metric was applied to a single frame and to the average of all frames. Significant improvements were achieved on all components of the image stack. The approximation ('Dc') showed better values of I_{ratio} than the full SeDDaRA theory ('Dx'). This suggests a better reference can be found if the analyst believes more improvement is likely. However, visual inspection of the results suggests that the difference is minimal and the approximation can be used.

The collapsed frame of deconvolved images is shown in Figure 3(bottom). Using the same contrast settings as Figure 3(top), the filaments in the red segment of the processed image are visibly thinner and better defined, while the green points are brighter and sharper.

4.2 Image Stack Beta

A second set, called class series on the NIH web site, consisted of 25 layers, also consisting of 8-bit red and green layers, and has significantly more image blur. The averaged view and processed result are shown in Figure 6. No further information about either the collection process or the objects is provided.

Profile plots were created across sixteen image features to apply the image metric. For a FWHM average of 12.52 pixels, the processing of the red frames produced an improvement of 0.521 for the constant frequency approximation

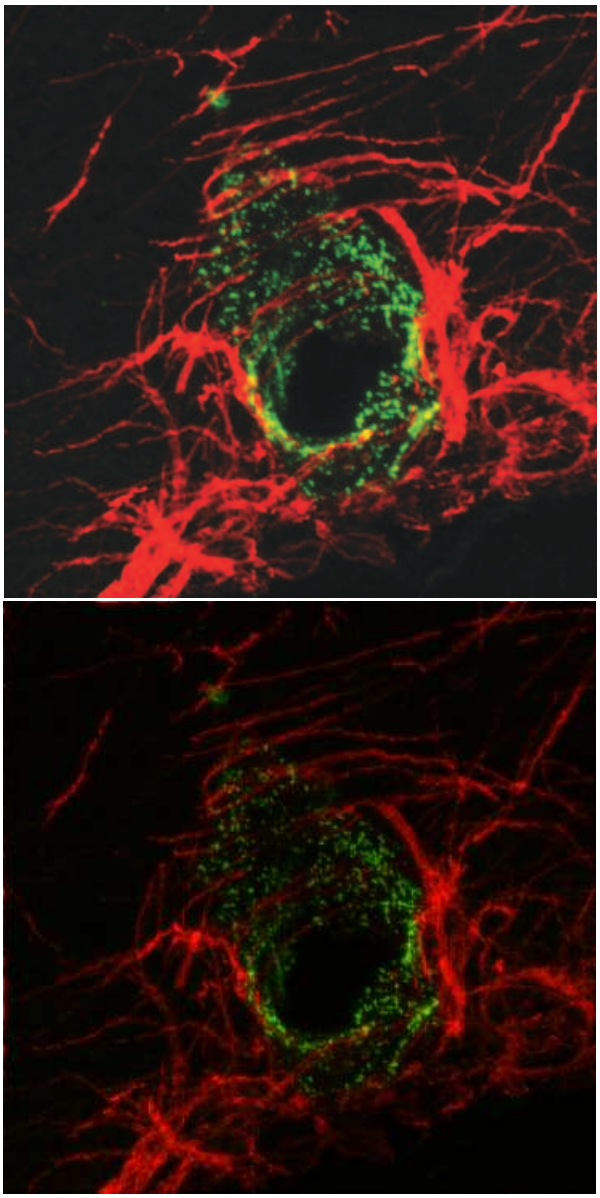

Figure 3: (Top) The averaged image from 36 frames from confocal stack alpha before processing. (Bottom) The averaged image of 36 deconvolved frames from the confocal stack using the constant-frequency approach. Image contrast has been improved and increased resolution is apparent.

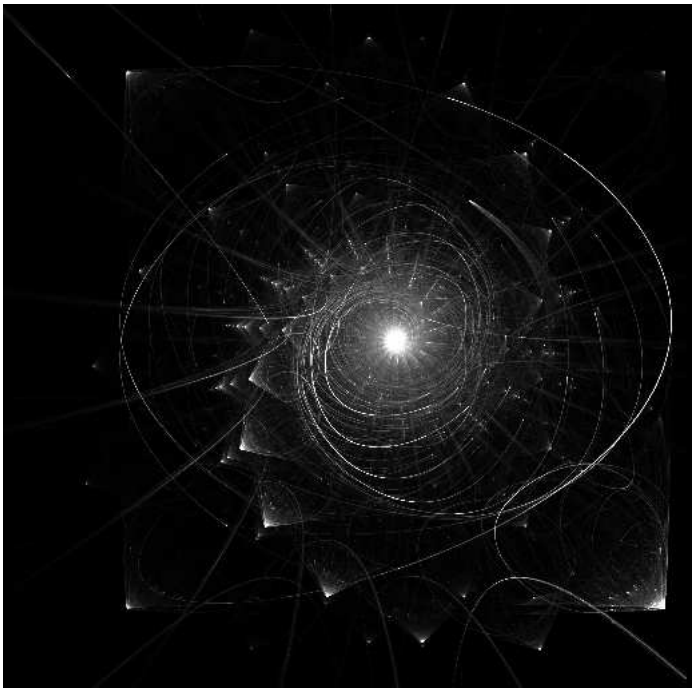

Figure 4: This fractal image was chosen as the reference image for processing the confocal stack using SeDDaRA.

	FWHM Orig.	FWHM Dc	FWHM Dx	I_{ratio} Dc	I_{ratio} Dx
Red Single	3.39	2.63	2.76	0.223	0.188
Red Ave.	4.34	3.29	3.49	0.242	0.196
Green Single	3.62	2.93	2.78	0.234	0.190
Green Ave.	5.32	4.08	4.51	0.233	0.151

Table 1: Image Metric results for confocal stack alpha. The first three columns are the average of the FWHM of sixteen image features in pixels. The last two columns show the improvement ratio when images are processed using the constant-frequency approximation ('Dc') and the full SeDDaRA theory ('Dx').

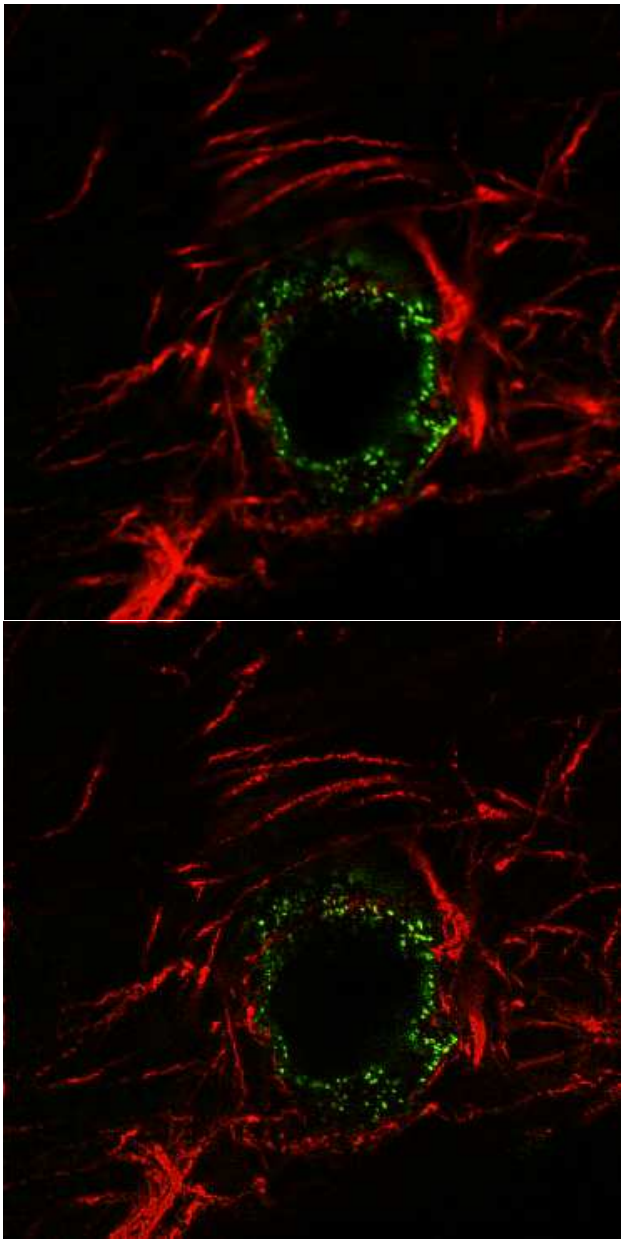

Figure 5: The top image is frame 20 of the NIH confocal image stack. The constant-frequency approximation of SeDDaRA was applied with $\alpha = 0.4$ to remove the blur from the image.

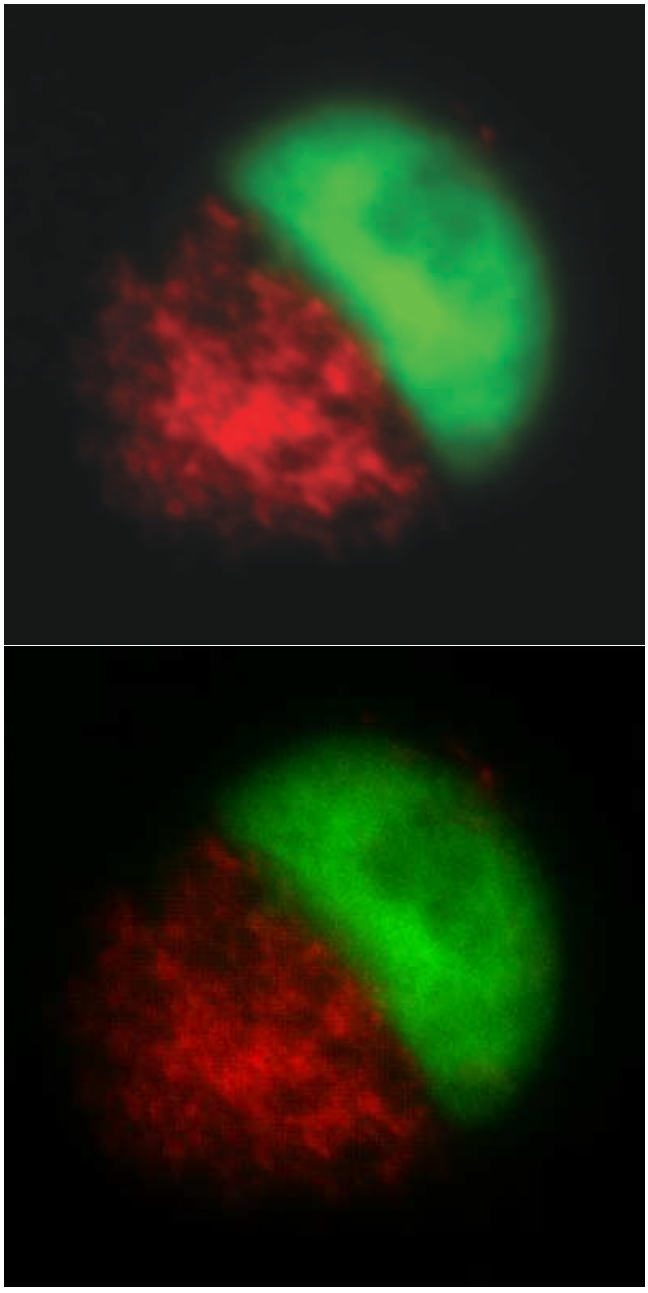

Figure 6: (Top) The collapsed image of 25 frames from a confocal stack. (Bottom) The collapsed image of 25 deconvolved frames from a confocal stack processed using SeDDaRA.

and 0.570 for SeDDaRA. Due to the lack of small features in the green frames, the metrics could not be applied.

5 Conclusions

This paper described the application of the SeDDaRA blind deconvolution method and the constant-frequency approximation to image stacks created by confocal microscopic imaging. Being non-iterative, this technique is considerably more computationally efficient than commonly-used iterative methods. Visual inspection of the processed images reveal significant improvements in image resolution. To quantify the effectiveness, a resolution improvement metric, based on the full-width half maximum value of image features, was described and applied to the results of the processing. In the two cases, considerable improvements were produced in the resolution of both single frames and the combined averaged image. The metric also showed that constant-frequency approximation of SeDDaRA works as well as applying the full theory. This is important since it allows the analyst to forego finding a suitable reference image for application of SeDDaRA.

6 Author's Comments

This paper was not accepted for publication, but has been through the peer-review process. Revisions have been made in response to address the reviewer's comments. However, the reviewer requested that we provide additional knowledge of the image sets which was not available. As we are unable to produce our own set of confocal microscopic image stacks, we decided to offer the paper as a technical note. We do welcome future collaborations that will fulfill this request and produce a more complete paper.

References

[1] N. L. Dey , L. Blanc-Fraud, C. Zimmer, Z. Kam, P. Roux, J. C. Olivo-Marin, and J. Zerubia,"Richardson-Lucy algorithm with total variation regularization for 3D confocal microscope deconvolution," Microsc. Res. Tech. **69**, 260–266 (2006).

[2] J. Boutet de Monvel, S. Le Calvez, and M. Ulfendahl,"Image restoration for confocal microscopy: improving the limits of deconvolution. with application to the visualization of the mammalian hearing organ," Biophys. J. **80**, 2455–2470 (2001).

[3] T.J. Holmes, "Blind deconvolution of quantum-limited incoherent imagery: maximum-likelihood approach," J. Opt. Soc. Am. A. **9**, 1052–1061 (1992).

[4] P. Pankajakshan, B. Zhang, L. Blanc-Fraud, Z. Kam, J.-C. Olivo-Marin, and J. Zerubia,"Blind deconvolution for thin-layered confocal imaging," Appl. Opt. **48**, 4437–4448 (2009).

[5] L. Vega-Alvarado, I, Elezgaray, A. Hmar, M. Menard, C. Ranger, and G. Corkidi, "A comparison of image deconvolution algorithms applied to the detection of endocytic vesicles in fluorescence images of neural proteins," Conf. Proc. IEEE Eng. Med. Biol. Soc., 755–8 (2007).

[6] Y. Sudo, N. Baba, N. Miura, S. Ueno, and R. Kitai, "Application of self-deconvolution method to shift-and-add solar imaging," Appl. Opt. **45**, 2707-2710 (2006).

[7] H. Zuo, Q. Zhang, and R. Zhao, "An efficiency restoration method for turbulence-degraded image base on improved SeDDaRA method," Proc. SPIE. **7383**. 738341 (2006).

[8] W.E. Vanderlinde, and J.N. Caron, "Blind Deconvolution of SEM Images," Proceedings of the 33rd International Symposium for Testing and Failure Analysis, 97–102 (2007).

[9] E.S. Barriga , G. Erry, S. Yang, S. Russell, B. Raman, and P. Soliz, "Application of adaptive optics in retinal imaging: A quantitative and clinical comparison with standard cameras," Proceedings of SPIE **5688**, 152–163 (2005).

[10] J.N. Caron, N.M. Namazi, and C.J. Rollins, "Noniterative blind data restoration by use of an extracted filter function," Appl. Opt. **41**(32), 6884–6889 (2002).

[11] A.K. Jain, *Fundamentals of Digital Image Processing*, (Prentice-Hall. Englewood Cliffs, NJ, 1989).

[12] N. Wiener, *The Extrapolation, Interpolation, and Smoothing of Stationary Time Series with Engineering Applications*, (Wiley, New York, 1949).

[13] C.W. Helstrom, "Image Restoration by the Method of Least Squares," J. Opt. Soc. Am. 57:297–303 (1967).

[14] D. Slepian, "Linear Least-Squares Filtering of Distorted Images," J. Opt. Soc. Am. 57:918–919 (1967).

[15] J. R. Fienup, D. Griffith, L Harrington, A. M. Kowalczyk, J. J. Miller, and J. A. Mooney, "Comparison of Reconstruction Algorithms for Images from Sparse-Aperature Systems," Proc. SPIE. **4792**, 1–8 (2002).

[16] C. C. Cunningham, and D. Anthony, "Image Deconvolution of Extended Objects: A Comparison of the Inverse Fourier and the Lucy Techniques," Icarus. **102**(2), 307–315 (1993).

[17] G.R. Ayers, and J.C. Dainty, "Iterative blind deconvolution method and its application," Opt. Lett. **13**, 547–549 (1988).

[18] D.G. Sheppard, B.R. Hunt, and M.W. Marcellin, "Iterative multiframe superresolution algorithms for atmospheric-turbulence-degraded imagery," J. Opt. Soc. Am. A. Vol. **15**(4), 978–992 (1998).

[19] D. Kundur, and D. Hatzinakos, " A novel blind deconvolution scheme for image restoration using recursive filtering," IEEE Transcations on Signal Processing. **46**(2), 375–390 (1998).

[20] T.J. Schulz, "Multiframe blind deconvolution of astronomical images," J. Opt. Soc. Am. A. **10**(10), 1064–1073 (1993).

[21] A.S. Carasso, "Direct Blind Deconvolution," SIAM Journal of Applied Mathematics. **61**(6), 1980–2007 (2001).

[22] J.N. Caron, N.M. Namazi, R.L. Lucke, C.J. Rollins, and P.R. Lynn, Jr. . "Blind data restoration with an extracted filter function," Opt. Lett. **26**(15), 1164–1166 (2001).

[23] I. Avcibas, B. Sankur and K. Sayood, "Statistical evaluation of image quality measures. J. of Electronic Imaging," **11**, 206–223 (2002).

[24] R. Perko, A. Klaus, and M.l Gruber, "Quality comparison of digital and film-based images for photogrammetric purposes," ISPRS Commission III: Theory and Algorithms, 1136–1140 (2004).

[25] C. Mackay, J. Baldwin, N. Law, and P. Warner, "High resolution imaging in the visible from the ground without adaptive optics: new techniques and results," Proc. SPIE. **5492**, 128–135 (2004).

[26] National Institute of Health. ImageJ Example Images. Available at http://rsb.info.nih.gov/ij/images/.